# Modulation of $\pi$ -stacking modes and photophysical properties of an organic semiconductor through isosteric cocrystallization

Cite as: J. Chem. Phys. 155, 071102 (2021); doi: 10.1063/5.0059770

Submitted: 11 June 2021 • Accepted: 3 August 2021 •

Published Online: 17 August 2021







Gonzalo Campillo-Alvarado,<sup>1,a)</sup> [b] Michael Bernhardt, Daniel W. Davies, <sup>1</sup> [b] Julio A. N. T. Soares, <sup>2</sup> Toby J. Woods, <sup>3</sup> [b] and Ying Diao 1 [b]

# **AFFILIATIONS**

- <sup>1</sup> Department of Chemical and Biomolecular Engineering, University of Illinois Urbana-Champaign, 600 S. Mathews Avenue, Urbana, Illinois 61801, USA
- <sup>2</sup> Frederick Seitz Materials Research Laboratories Central Facilities, University of Illinois Urbana-Champaign, 104 South Goodwin Avenue, Urbana, Illinois 61801, USA
- School of Chemical Sciences, University of Illinois Urbana-Champaign, 505 S. Mathews Avenue, Urbana, Illinois 61801, USA

Note: This paper is part of the 2021 JCP Emerging Investigators Special Collection.

a) Author to whom correspondence should be addressed: gcampi@illinois.edu

# **ABSTRACT**

We report on the control of  $\pi$ -stacking modes (herringbone vs slipped-stack) and photophysical properties of 9,10-bis((E)-2-(pyridin-4-yl)vinyl)anthracene (**BP4VA**), an anthracene-based organic semiconductor (OSC), by isosteric cocrystallization (i.e., the replacement of one functional group in a coformer with another of "similar" electronic structure) with 2,4,6-trihalophenols (**3X-ph-OH**, where X = Cl, Br, and I). Specifically, **BP4VA** organizes as slipped-stacks when cocrystallized with **3Cl-ph-OH** and **3Br-ph-OH**, while cocrystallization with **3I-ph-OH** results in a herringbone mode. The photoluminescence and molecular frontier orbital energy levels of **BP4VA** were effectively modulated by the presence of **3X-ph-OH** through cocrystallization. We envisage that the cocrystallization of OSCs with minimal changes in cocrystal formers can provide access to convenient structural and property diversification for advanced single-crystal electronics.

Published under an exclusive license by AIP Publishing. https://doi.org/10.1063/5.0059770

# INTRODUCTION

Emerging developments in the design of crystalline organic semiconductors (OSCs) have paved the way to engineer next-generation electronics. <sup>1,2</sup> Namely, strategies to enhance charge transport in crystalline OSCs rely on achieving an efficient  $\pi$ -stacking between adjacent molecules to maximize orbital overlap. <sup>3,4</sup> While strategies to optimize  $\pi$ -stacking in OSCs have mainly relied on covalent modification and derivatization (e.g., single-atom substitution, <sup>5–7</sup> addition of bulky groups, <sup>8</sup> extension of aromatic cores, <sup>9,10</sup> and B-coordination <sup>11</sup>), supramolecular strategies (i.e., cocrystallization <sup>12–18</sup>) to diversify and control crystal packing are a largely uncharted territory.

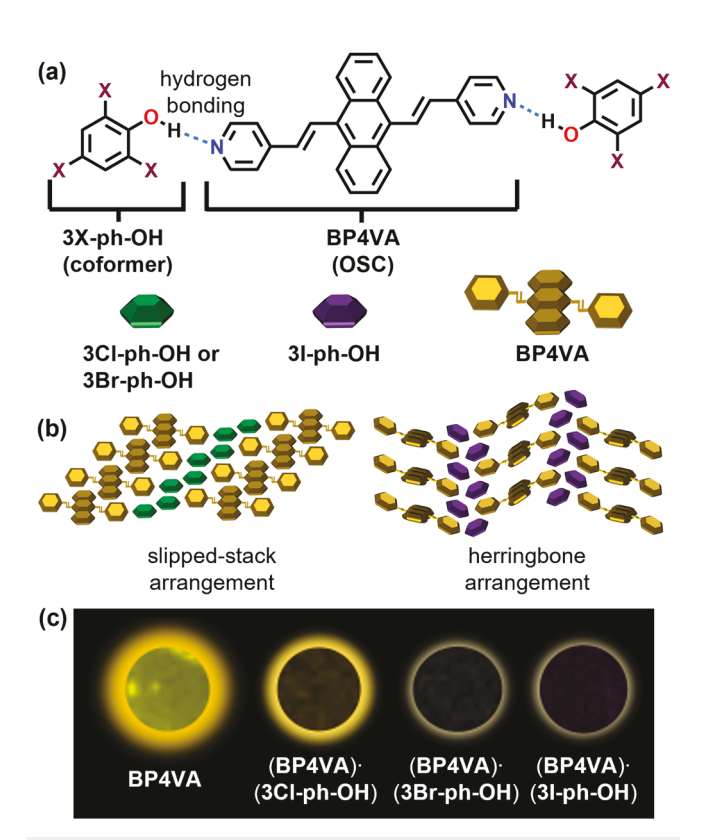
Recent examples of supramolecular derivatization of OSCs involve the encapsulation of  $C_{70}$  with buckybowls<sup>19</sup> and  $\pi$ -stacked

complexes through cocrystallization. Although cocrystallization has been exploited to enforce the face-to-face  $\pi$ -stacking of OSCs in discrete systems, trategies to modulate the overall extended packing modes/motifs (e.g., lamellar, herringbone, and slipped  $\pi$ -stacks) 4.21.22 of organic semiconductors have not been explored to the best of our knowledge.

Herein, we report the modulation of extended packing modes (herringbone vs slipped-stack) of 9,10-bis((E)-2-(pyridin-4-yl)vinyl)anthracene (**BP4VA**),<sup>23,24</sup> an OSC widely employed in optoelectronics. Pristine **BP4VA** employed in this study crystallizes in the monoclinic system  $P2_1/c$ , adopting a staircase-type aggregation along the b-axis sustained by the strong face-to-face  $[\pi \cdots \pi]$  stacking of anthracene cores. Additional  $[C-H\cdots N]$  contacts sustain the aggregates in the ac-plane (see Fig. S3 in the supplementary material).<sup>23</sup> It has been previously discussed that

the low-lying intramolecular Highest Occupied Molecular Orbital (HOMO)–Lowest Unoccupied Molecular Orbital (LUMO) transition is primarily related to the anthracene core and that the arrangement of the anthracene planes could play a key role in controlling photoluminescence (PL) in solids.<sup>23</sup> The modulation of packing of **BP4VA** is achieved through isosteric cocrystallization (i.e., replacement of a functional group in the coformer with another of similar electronic structure)<sup>25–27</sup> with a family of 2,4,6-trihalophenols (**3X-ph-OH**, where X = Cl, Br, and I) [Schemes 1(a) and 1(b)]. The cocrystals effectively modulate photophysical properties [i.e., photoluminescence (PL) and optical bandgap] [Scheme 1(c)].

Specifically, we show **BP4VA** to crystallize in slipped-stack arrangement with **3Cl-ph-OH** and **3Br-ph-OH**, while cocrystallization with **3I-ph-OH** results in an overall herringbone arrangement. Herringbone packing is sustained primarily by robust  $[C-I \cdots \pi]$  contacts<sup>28,29</sup> from **3I-ph-OH** coformers. The cocrystallization of **BP4VA** with **3X-ph-OH** results in the modulation of relative PL intensities and HOMO–LUMO and optical gaps.<sup>30</sup> To the best of our knowledge, we are unaware of a systematic cocrystallization study of an OSC with isosteric coformers. The ability to modulate the overall extended packing modes/motifs and photophysical properties of an OSC with isosteric cocrystallization is also demonstrated.



SCHEME 1. Modulation of crystal packing and photoluminescence of BP4VA based on isosteric cocrystallization: (a) three-component assembly of (BP4VA)·2(3X-ph-OH), where X = Cl, Br, and I; (b) slipped-stack and herring-bone arrangements of cocrystals; and (c) relative photoluminescence intensity of cocrystals and pure BP4VA.

### **METHODS**

Our strategy to influence the extended packing modes of BP4VA using isosteric cocrystallization involved the addition of 15 mg of BP4VA (0.039 mmol) to the corresponding 3X-ph-OH (0.078 mmol) in 3 ml of a binary solvent mixture [3:1 (v/v) chloroform/acetonitrile]. The solutions were sonicated for 10 s and gently heated until all the components dissolved. Slow evaporation of the solutions afforded single crystals after a period of 2–3 days as yellow plates for (BP4VA)·2(3Cl-ph-OH) and (BP4VA)·2(3Cl-ph-OH) and red plates for (BP4VA)·2(3I-ph-OH). Cocrystal formulations were confirmed by single-crystal x-ray diffraction (SCXRD) and powder x-ray diffraction (PXRD) (see the supplementary material).

# **RESULTS AND DISCUSSION**

SCXRD analysis revealed the components of (BP4VA). 2(3Cl-ph-OH) to crystallize in the triclinic space group P-1 as discrete three-component assemblies sustained via two  $[O-H\cdots N]$  hydrogen bonds [Fig. 1(a)]. The anthracenyl core lies twisted out from the pyridyl rings (twist angle: 61.8°). The halophenyl rings from 3Cl-ph-OH also lie significantly twisted in relation with the pyridyl rings (73.4°) and nearly coplanar with the anthracenyl core (11.9°).

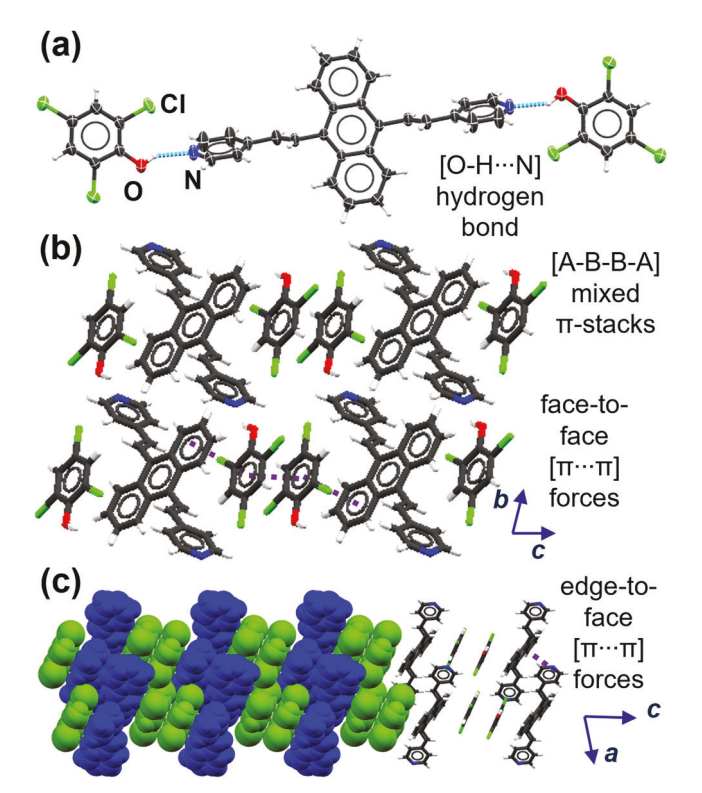


**FIG. 1.** Crystal structure of (**BP4VA**)·2(3**CI-ph-OH**): (a) three-component assembly sustained by hydrogen bonds (thermal ellipsoids at the 50% probability level), (b) mixed stacks along the c-axis sustained by face-to-face  $[\pi \cdots \pi]$  contacts, and (c) parallel stacks along the a-axis interacting through edge-to-face  $[\pi \cdots \pi]$  contacts.

The components form 1D mixed stacks of an [A-B-B-A]<sub>n</sub> pattern (A = **BP4VA** and B = **3Cl-ph-OH**), which run along the crystallographic *c*-axis sustained by face-to-face  $[\pi \cdots \pi]$  interactions [Fig. 1(b)]. Additional edge-to-face  $[\pi \cdots \pi]$  interactions between the pyridyl ring and anthracenyl core of **BP4VA** connect the 1D stacks [Fig. 1(c)] as wrinkled layers in the *ac*-plane. Overall, the crystal packing arrangement is defined as a slipped-stack arrangement as determined by the main  $\pi$ -stacking direction. Cocrystal (**BP4VA**) 2(3**Br-ph-OH**) was deemed isostructural to (**BP4VA**)·2(3**Cl-ph-OH**) by SCXRD analysis and close agreement of simulated PXRD patterns (similarity index = 96.1%), single crystal unit cell parameters, and geometry (see the supplementary material).

The formation of a herringbone packing mode was evidenced in the cocrystals of (BP4VA)·2(3I-ph-OH). Specifically, SCXRD analysis revealed the components to crystallize in the monoclinic space group  $P2_1/c$  as a hydrogen-bonded three-component assembly [Fig. 2(a)]. The anthracenyl core and pyridyl rings lie significantly less twisted (twist angle: 57.4°) than (BP4VA)·2(3Cl-ph-OH) and (BP4VA)·2(3Br-ph-OH). Notably, the halophenyl rings sit almost orthogonally to the anthracenyl ring (80°) compared to the previous cases, wherein the halophenyl and anthracenyl rings are almost coplanar. The extended herringbone motif is primarily sustained by  $[C-I\cdots\pi]$  contacts between adjacent halophenols and faceto-face  $[\pi\cdots\pi]$  interactions with the anthracenyl core [Fig. 2(b)]. The observation is in agreement with a recent survey of crystal

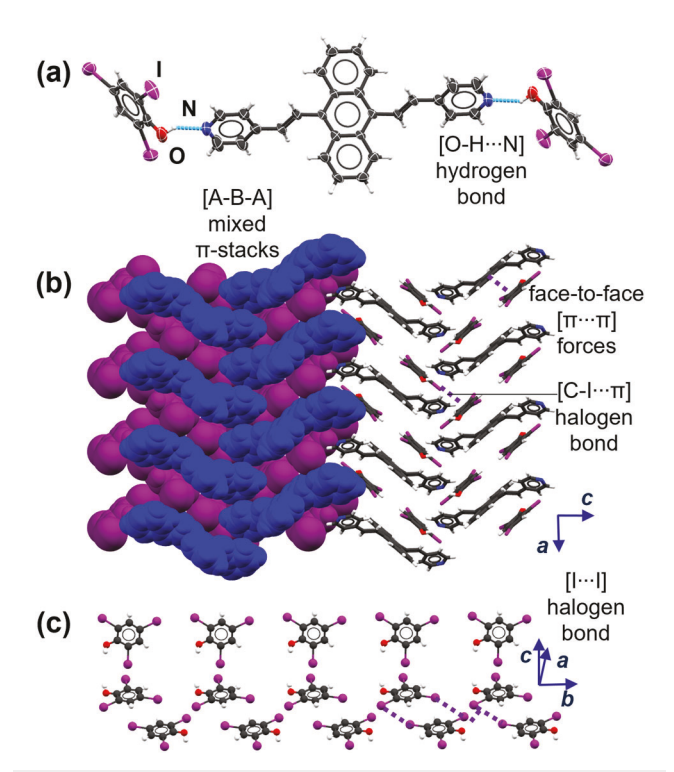


**FIG. 2.** Crystal structure of (**BP4VA**)-2(**3I-ph-OH**): (a) three-component assembly sustained by hydrogen bonds (thermal ellipsoids at the 50% probability level), (b) the combination of  $[C-l\cdots\pi]$  and face-to-face  $[\pi\cdots\pi]$  contacts sustain a herringbone packing, and (c) the array of **3I-ph-OH** molecules sustained by halogen bonds (**BP4VA** molecules are omitted for clarity).

structures containing  $[C-X\cdots\pi]$  contacts, where X = Cl, Br, and I, which indicated that  $[C-I \cdots \pi]$  exhibits an increased likelihood to form and serve as structure-directing. The origin of  $[C-X\cdots\pi]$ contacts is mainly dispersive with small contributions from Coulombic attraction and charge-transfer.<sup>28</sup> In addition, the halophenol molecules in (BP4VA)·2(3I-ph-OH) engage with type II [I···I] halogen bonds  $[(\theta_1 \simeq 180^{\circ} \text{ and } \theta_2 \simeq 90^{\circ})$ , where  $\theta_1$  and  $\theta_2$  are the C-X···X' and C-X'···X angles (where X and X' = Cl, Br, and I)] $^{31,32}$  in the crystal lattice [Fig. 2(c)]. The overall packing is reminiscent of 2D supramolecular J-dimer lamellae formed by iodinated BODIPY (boron dipyrromethene) dyes.<sup>33</sup> The Hirshfeld surface analysis of cocrystals confirms the increased population of  $[X \cdot \cdot \cdot C]$ interactions in (BP4VA) 2(3I-ph-OH) compared to isostructural cocrystals (BP4VA)·2(3Cl-ph-OH) and (BP4VA)·2(3Br-ph-OH), which favor a herringbone mode through the orthogonal reorganization of halophenols (see the supplementary material for Hirshfeld interaction contributions). Contrary to the molecular arrangement in the pristine crystals of BP4VA, we note that no direct face-to-face  $[\pi \cdots \pi]$  interactions between the anthracene cores of BP4VA molecules were observed in the cocrystal series.

Profound changes in the photophysical properties of BP4VA are also observed as a result of isosteric cocrystallization. Specifically, the single crystals of pure BP4VA are highly photoluminescent (under 488 nm excitation) with a PL peak ( $\lambda_{max}$ ) at ~540 nm. Relative PL intensity in cocrystals gradually decreases from Cl (reduced PL) to Br ≈ I (notably reduced PL), in agreement with the "heavy-atom effect" (i.e., fluorescence quenching due to the enhancement of radiative and nonradiative intercombination transitions) caused by the presence of halophenols, with iodide being the most efficient quencher and chloride the least effective.<sup>34-3</sup> Since the majority of the HOMO-LUMO orbitals are located in the anthracene core (vide infra), changes in PL intensity could also be attributed as a result of close intermolecular contacts of the anthracene core with neighboring halophenols (i.e., face-toface  $[\pi \cdot \cdot \cdot \pi]$  stacking) and modifications of the overall  $\pi$ -stacking modes. The modulation of PL is reminiscent of modulation of solidstate photoactivity in the cocrystals of halophenols with 1,2-bis(4pyridyl)ethylene.<sup>37</sup> While the PL spectrum of (BP4VA)·2(3Cl-ph-**OH**) showed a blueshift of ~18 nm ( $\lambda_{\text{max}} = 522$  nm), the spectra of (BP4VA)·2(3Br-ph-OH) and (BP4VA)·2(3I-ph-OH) showed a redshift of ~135 and 90 nm, respectively [Figs. 3(a) and 3(b)]. The redshift of (BP4VA)·2(3Br-ph-OH) and (BP4VA)·2(3I-ph-OH) is in agreement with less torsion angles of the bonds connecting the anthracene core and pyridyl rings of cocrystals compared to those of (BP4VA)-2(3Cl-ph-OH) (see Fig. S4 in the supplementary material). Less torsion (i.e., stronger  $\pi$ -conjugation and  $\pi$ -stacking of BP4VA molecules with halophenols) might contribute to a long emission wavelength because of a strong exciton couple as observed elsewhere.14,38

The UV–vis spectra of **BP4VA** and cocrystals showed absorption peaks ( $\lambda_{max}$ ) in the range of 400–500 nm [Fig. 3(c)]. The direct optical gaps of materials were calculated from Tauc analyses of UV–vis spectra (see Table S3 in the supplementary material). It was noted that the optical gap of (**BP4VA**)·2(3**I-ph-OH**) (2.481 eV) was narrower than that of pure **BP4VA** (2.526 eV), while the gaps of (**BP4VA**)·2(3**Cl-ph-OH**) and (**BP4VA**)·2(3**Br-ph-OH**) were slightly wider (2.560 and 2.567 eV, respectively) [Fig. 3(d)].

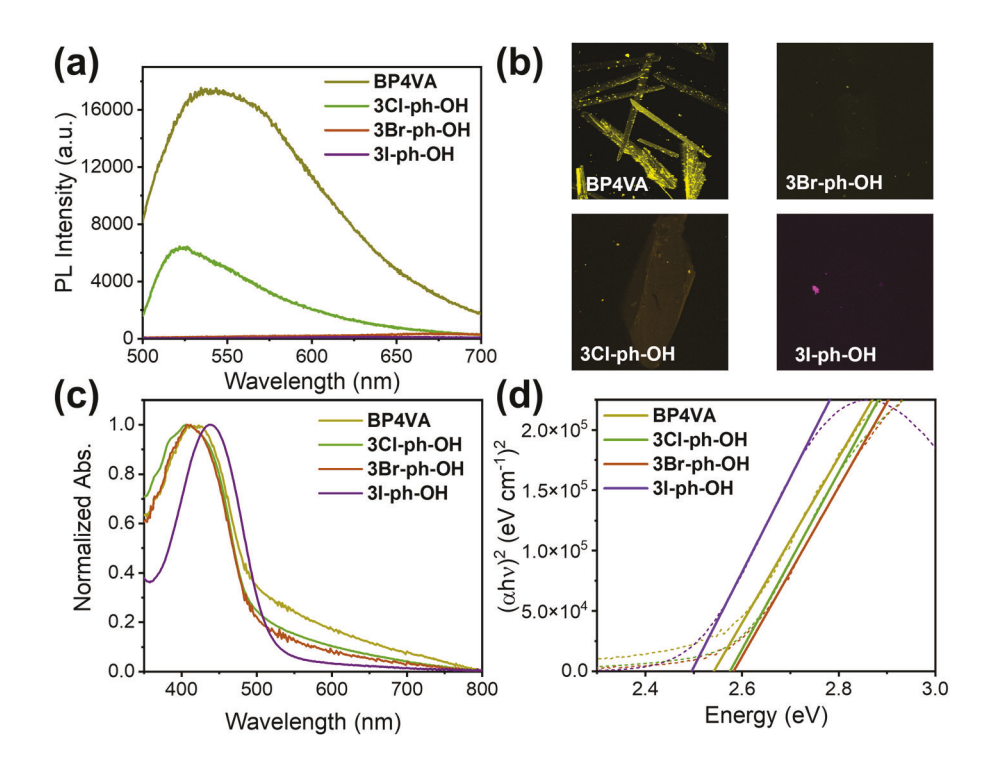


FIG. 3. Photophysical properties of BP4VA and cocrystals: (a) PL spectra showing relative intensities, (b) confocal fluorescence microscopy photographs of single crystals, (c) UV–vis absorption spectra, and (d) Tauc plots highlighting optical gaps. The cocrystals are labeled with the corresponding coformer.

To gain a better understanding of the modulation of the optical gaps using isosteric cocrystallization, time-dependent density-functional theory (TD-DFT) calculations (6-311G++ basis set) using crystallographic coordinates were performed for **BP4VA** and the cocrystal series to visualize the Highest Occupied Molecular Orbital (HOMO) and Lowest Unoccupied Molecular Orbital

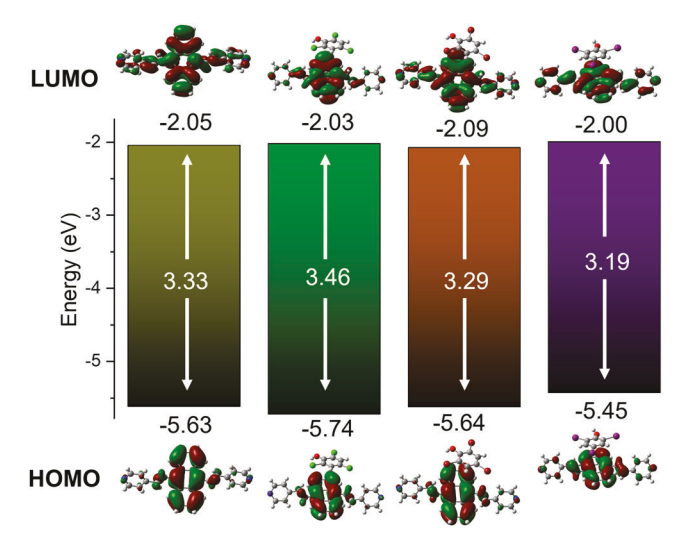


FIG. 4. HOMO–LUMO energy diagram and frontier molecular orbitals of BP4VA and cocrystals (BP4VA)-2(3CI-ph-OH), (BP4VA)-2(3Br-ph-OH), and (BP4VA)-2(3X-ph-OH). The bottom bars represent the HOMO energy, and the top bars represent the LUMO energy. The HOMO–LUMO energy gaps are shown in the middle.

(LUMO). UV–vis spectral simulations (see Fig. S10 in the supplementary material) were comparable to experimental data, and HOMO–LUMO gaps were in close agreement with optical gaps. Generally, molecular orbitals at HOMO levels are located mainly in the anthracene core, while delocalization promoted by the electron-deficient pyridyl ring partially distributes electron density over the molecule at LUMO levels. The formation of hydrogen bonding and  $\pi$ -staking of **BP4VA** with halophenols could promote the stabilization of LUMO levels as previously observed in the protonation studies of **BP4VA** and structural isomers (Fig. 4).<sup>23,39,40</sup>

# CONCLUSION

We have demonstrated that the crystal packing modes and photophysical properties of **BP4VA** can be readily modulated through isosteric cocrystallization with 2,4,6-trihalophenols as hydrogenbonded aggregates. On the one hand, an overall slipped-stack architecture is promoted in (**BP4VA**) 2(3**Cl-ph-OH**) and (**BP4VA**) 2(3**Br-ph-OH**) primarily through face-to-face  $[\pi \cdots \pi]$  and edge-to-face  $[\pi \cdots \pi]$  interactions. On the other hand, the orthogonal geometry of 3**I-ph-OH** in (**BP4VA**) 2(3**I-ph-OH**) caused by  $[C-I \cdots \pi]$  contacts enables a herringbone packing mode. The photophysical properties (e.g., PL, UV-vis absorption, and bandgap) of **BP4VA** are also modulated through small changes in the cocrystal former. We envisage that the isosteric cocrystallization of OSCs could be implemented to diversify and fine tune optical and electronic properties without the need to redesign and synthesize covalent analogs.

# SUPPLEMENTARY MATERIAL

See the supplementary material for detailed information on materials and experimental methods, complete crystallographic data, polarized optical microscopy data, molecular modeling data, and photophysical data.

### **ACKNOWLEDGMENTS**

G.C.-A. acknowledges financial support from The Office for Access and Equity, the DRIVE Committee, and the Illinois Materials Research Center (University of Illinois at Urbana-Champaign) through the DRIVE Distinguished Postdoctoral Fellowship. Y.D. and D.W.D. acknowledge the Sloan Foundations for a Sloan Research Fellowship in Chemistry and a 3M Nontenured Faculty Award. This work was conducted, in part, in the George L. Clark X-Ray Facility and in the 3M Materials Laboratory and in the Materials Research Laboratory Central Research Facilities, University of Illinois. This research was partially supported by the NSF through the University of Illinois at Urbana-Champaign Materials Research Science and Engineering Center under Grant No. DMR-17-20633. The use of the Advanced Photon Source, an Office of Science User Facility operated for the U.S. Department of Energy (DOE) Office of Science by Argonne National Laboratory, was supported by the U.S. DOE under Contract No. DE-AC02-06CH11357. We are thankful to Dr. Danielle L. Gray (University of Illinois), Dr. Yu-Sheng Chen (ChemMatCARS), Dr. Tievan Chang (ChemMat-CARS), Dr. Ying-Pin Chen (ChemMatCARS), and Dr. SuYin Grass Wang (ChemMatCARS) for assistance with SCXRD measurements.

There are no conflicts of interest to declare.

### DATA AVAILABILITY

The data that support the findings of this study are openly available in The Cambridge Crystallographic Data Centre (CCDC Nos.: 2081468, 2081468, and 2081470).

# **REFERENCES**

```
<sup>3</sup>R. M. Pinto et al., J. Am. Chem. Soc. 137, 7104 (2015).
```

<sup>&</sup>lt;sup>1</sup>X. Zhang, H. Dong, and W. Hu, Adv. Mater. 30, 1801048 (2018).

<sup>&</sup>lt;sup>2</sup>L. Sun et al., Mater. Chem. Front. 4, 715 (2020).

<sup>&</sup>lt;sup>4</sup>Z.-F. Yao, J.-Y. Wang, and J. Pei, Cryst. Growth Des. 18, 7 (2018).

<sup>&</sup>lt;sup>5</sup>J.-H. Dou et al., J. Am. Chem. Soc. **137**, 15947 (2015).

<sup>&</sup>lt;sup>6</sup>J. E. Anthony, Angew. Chem., Int. Ed. 47, 452 (2008).

<sup>&</sup>lt;sup>7</sup>Y. J. Bae et al., J. Chem. Phys. **151**, 044501 (2019).

<sup>&</sup>lt;sup>8</sup>Q. Miao et al., J. Am. Chem. Soc. 128, 1340 (2006).

<sup>&</sup>lt;sup>9</sup>C. Aumaitre and J. F. Morin, Chem. Rec. **19**, 1142 (2019).

<sup>&</sup>lt;sup>10</sup>C. Wang et al., Chem. Sci. 11, 1573 (2020).

<sup>&</sup>lt;sup>11</sup>G. Campillo-Alvarado et al., Cryst. Growth Des. 21, 3143 (2021).

<sup>&</sup>lt;sup>12</sup>P. Yu et al., Chem 5, 2814 (2019).

<sup>&</sup>lt;sup>13</sup> K. K. Ray et al., Cryst. Growth Des. **20**, 3 (2020).

<sup>&</sup>lt;sup>14</sup>L. Sun et al., Adv. Mater. **31**, 1902328 (2019).

<sup>&</sup>lt;sup>15</sup>C. Gozálvez et al., Chem. Sci. 10, 2743 (2019).

<sup>&</sup>lt;sup>16</sup>G. Campillo-Alvarado et al., Cryst. Growth Des. 18, 4416 (2018).

<sup>&</sup>lt;sup>17</sup>G. Campillo-Alvarado et al., CrystEngComm 19, 2983 (2017).

<sup>&</sup>lt;sup>18</sup>G. Campillo-Alvarado et al., CrystEngComm 22, 3563 (2020).

<sup>&</sup>lt;sup>19</sup>G. Gao et al., J. Am. Chem. Soc. **142**, 2460 (2020).

<sup>&</sup>lt;sup>20</sup> A. N. Sokolov, T. Friščić, and L. R. MacGillivray, J. Am. Chem. Soc. 128, 2806

<sup>&</sup>lt;sup>21</sup>C. Wang et al., Cryst. Growth Des. **10**, 4155 (2010).

<sup>&</sup>lt;sup>22</sup>Y.-Y. Lai et al., ACS Omega 3, 18656 (2018).

<sup>&</sup>lt;sup>23</sup>Y. Dong et al., J. Mater. Chem. C 1, 7554 (2013).

<sup>&</sup>lt;sup>24</sup>S. Ma et al., J. Phys. Chem. Lett. **8**, 3068 (2017).

<sup>&</sup>lt;sup>25</sup>D. P. Ericson et al., Cryst. Growth Des. **15**, 5744 (2015).

<sup>&</sup>lt;sup>26</sup> K. M. Hutchins et al., Supramol. Chem. **30**, 533 (2018).

<sup>&</sup>lt;sup>27</sup>L. T. Sein, Y. Wei, and S. A. Jansen, J. Phys. Chem. A **104**, 11371 (2000).

<sup>&</sup>lt;sup>28</sup>E. R. T. Tiekink, CrystEngComm 23, 904 (2021).

<sup>&</sup>lt;sup>29</sup> J. Vainauskas et al., Chem. Commun. **56**, 15145 (2020).

<sup>&</sup>lt;sup>30</sup>J.-L. Bredas, Mater. Horiz. 1, 17 (2014).

<sup>&</sup>lt;sup>31</sup> P. Metrangolo and G. Resnati, IUCrJ 1, 5 (2014).

<sup>&</sup>lt;sup>32</sup> A. Mukherjee and G. R. Desiraju, IUCrJ 1, 49 (2014).

<sup>&</sup>lt;sup>33</sup>M. Su et al., Chem. Eur. J. 26, 4505 (2020).

<sup>&</sup>lt;sup>34</sup> K. N. Solov'ev and E. A. Borisevich, *Phys.-Usp.* **48**, 231 (2005).

<sup>35</sup> G. Cavallo et al., Chem. Rev. 116, 2478 (2016).

<sup>&</sup>lt;sup>36</sup>S. d'Agostino et al., Cryst. Growth Des. 15, 2039 (2015).

<sup>&</sup>lt;sup>37</sup>G. Campillo-Alvarado et al., Cryst. Growth Des. 19, 2511 (2019).

<sup>&</sup>lt;sup>38</sup>Y. Han et al., Cryst. Growth Des. **21**, 1342 (2021).

<sup>&</sup>lt;sup>39</sup> J. Zhang et al., Chem. Commun. **49**, 3878 (2013).

<sup>&</sup>lt;sup>40</sup>Y. Dong et al., Angew. Chem., Int. Ed. **51**, 10782 (2012).